



Contents lists available at ScienceDirect

Continental Shelf Research

journal homepage: www.elsevier.com/locate/csr

Quantifying mud settling velocity as a function of turbulence and salinity in a deltaic estuary

M. McDonnell^a, K. Strom^b, J. Nittrouer^c, G. Mariotti^{a,d,*}

^a College of the Coast and Environment, Louisiana State University, Baton Rouge, LA, 70803, USA

^b Civil and Environmental Engineering, Virginia Tech, Blacksburg, VA, 24061, USA

^c Department of Geosciences, Texas Tech University, Lubbock, TX, 79409, USA

^d Center for Computation and Technology, Louisiana State University, Baton Rouge, LA, 70803, USA

ABSTRACT

Mud settling velocity in coastal regions is controlled by flocculation, which in turn strongly depends on turbulence, chemistry, and biology of the water-sediment mixture. As a result, mud settling velocity can be poorly constrained, and vary in space and time by orders of magnitude. Here we quantified mud settling velocity in Barataria Basin, a deltaic estuary in Louisiana (USA), using three independent methods: eddy covariance (one station for 200 days), floc cameras (4 stations at one time), and Rouse profile inversion (14 stations, replicated 10–30 times each). Eddy covariance indicates that settling velocity increases with turbulence, at least within the range experienced at the site (shear rate G up to 10 Hz). Settling velocity increases with salinity (in the 0 to 6 psu range) for moderate turbulence levels ($5 < G < 10$ Hz), but it is nearly independent of salinity for low levels of turbulence ($G < 5$ Hz). Consistent with this finding, floc camera measurements – taken at low turbulence levels – indicate similar floc sizes for salinities from 0.4 to 20 psu. Settling velocity estimated from a Rouse profile inversion also lacks a dependence on salinity, likely because they were taken at low turbulence levels. This study is novel in that it utilizes three methodologies to independently predict the mud settling velocity, with quantified settling velocity values ranging 0.1–1 mm/s, and with most values between 0.2 and 0.5 mm/s. Overall these measurements confirm that mud is flocculated in both the saline and freshwater zones of Barataria Basin, and that turbulence is the largest factor controlling mud settling velocity. Nonetheless, salinity can increase mud settling velocity up to a factor of two. These results could inform the management of sediment imported into estuaries from freshwater sources, such as through natural drainages, crevasse splays, and engineered river diversions.

1. Introduction

Fine particles such as silt and clay – collectively referred to as mud – are highly abundant in estuaries and low-energy coastal areas. The settling velocity of mud is a crucial parameter for determining its transport and ultimate fate in these environments. For example, mud settling velocity strongly controls the distance at which mud is deposited from its original source. Mud with higher settling velocity is more likely to be retained within the estuary, and more specifically to be retained on the marsh platform (Voulgaris and Meyers, 2004), thus contributing to its vertical accretion.

Mud settling velocity depends on the flocculation state of the mud, which itself depends on the fluid turbulence and the chemical and biological characteristics of the water-sediment suspension. Flocculation refers to the process whereby individual clay and silt size inorganic and organic materials bind together to create aggregates or flocs that are larger in size than any of the individual constitutive particles. At low levels of turbulence, flocs have the potential to grow in size and form larger aggregates that can range in size from about 100 to 500 μm due to

the lower levels of hydrodynamic stress acting on the particle aggregates, thereby reducing floc breakup rates. However, in these low-shear settings, the flow cannot always keep the larger flocculated material in suspension. In such cases, larger particles and flocs settle from the water column, leaving smaller flocs or individual particles in suspension. At much higher levels of turbulence, the flow can keep material suspended, but floc size can be limited by the fluid stress acting on the aggregate. Hence, due to settling at lower turbulence levels and shear-limited floc growth at higher levels of turbulence, the largest flocs observed in the water column are usually present at intermediate levels of turbulence or bed shear stress (Winterwerp, 1998).

Water chemistry controls ion interactions which impact pH, salinity, and organic content, all of which can influence flocculation (Mietta et al., 2009). Increases in salinity have generally been associated with increased floc sizes, especially in the low salinity ranges (0–5 psu) (Al Ani et al., 1991; Abolfazli and Strom, 2023). Settling velocity rates can vary in estuaries and some studies have found that settling velocity can change drastically when salinity impacts flocculation of sediment (Mikeš and Manning, 2010). However, others have suggested that salinity plays

* Corresponding author. College of the Coast and Environment, Louisiana State University, Baton Rouge, LA, 70803, USA.

E-mail address: gmariotti@lsu.edu (G. Mariotti).

<https://doi.org/10.1016/j.csr.2024.105180>

Received 10 July 2023; Received in revised form 17 January 2024; Accepted 18 January 2024

Available online 19 January 2024

0278-4343/© 2024 Elsevier Ltd. All rights reserved.

a limited role in determining floc size relative to organic matter and hydrodynamics (Eisma, 1986; Thill et al., 2001; Verney et al., 2009).

Outside of a relatively small number of studies (e.g. Droppo et al., 1998; Droppo et al., 1998; Phillips and Walling, 1999; Fox et al., 2014; Le et al., 2020) flocculation in freshwater has been assumed to be a negligible component of mud dynamics. Recent analyses of mud concentration profiles have however pointed to the likely presence of flocs as the driver of vertical gradients in mud concentration profiles within large freshwater rivers (Izquierdo-Ayala et al., 2021; Lamb et al., 2020; Nghiem et al., 2022). In addition, recent *in situ* observations in the Mississippi River have shown that a significant fraction of the mud exists as floc aggregates (Osborn et al., 2021, 2023), likely due to the binding effect of organic matter (Mietta et al., 2009). Estimates of mud settling velocities from Rouse profile analysis (Lamb et al., 2020) and calculations from direct observations of floc size (Osborn et al., 2023) yield average mud floc settling velocities typically in the range of 0.1–1 mm/s – values sufficiently large to influence mud transport and deposition dynamics, and hence geomorphic evolution, relative to mud in an unflocculated state.

Models have been proposed to predict flocculation, for example by simulating turbulence-induced aggregation and breakup (Winterwerp et al., 2006a). In practice, however, flocculation (and hence settling velocity) is difficult to predict, and site-specific field measurements are needed to constrain it. Here we study mud settling velocity in Barataria Basin, a deltaic estuary in Louisiana (USA). Mud dynamics is particularly relevant in this estuary because of the proposed diversion of the Mississippi River (CPRA, 2017; Xu et al., 2016), which is expected to deliver up to 75,000 m³/s (CPRA, 2017) of water into Barataria. Within the middle areas of Barataria Basin, the location of the planned diversion, fine sediment (mud) is the most prevalent geological class while the southern part is sandier (Li et al., 2021). Given that mud constitutes 80–90% of the total sediment load in the Mississippi River (Nittrouer and Viparelli, 2014), predicting the fate of the mud entering Barataria through this diversion is essential to evaluate its benefits, i.e., its ability to reduce marsh loss (Xu et al., 2016).

Previous modeling studies of sediment dynamics in the estuaries and coastal areas of Louisiana have made strong assumptions about the mud settling velocity, and systematically neglected its dependence on turbulence or water chemistry. A study of the sediment plume of the Mississippi River (Sorourian et al., 2022), based on the FVCOM model, assumed that the settling velocity was 0.1 mm/yr for newly delivered mud and 3.4 mm/s for the mud already present in the bed. A study of the Mississippi Delta region, based on the COAWST model, assumed a settling velocity of 0.1 mm/yr for all mud particles (Zang et al., 2019). Studies focused on Barataria Basin (Baustian et al., 2018; Meselhe et al., 2021), based on the Delft3D model, assumed a settling velocity of 0.1 mm/s for silt and of 0.001 mm/s for clay – implicitly assuming that the clay was not flocculated. These uncertainties on these values directly translate to uncertainties in model predictions of mud deposition on the marsh surface.

Measuring the settling velocity of mud is complicated. Sediment can be composed of numerous physical and chemical properties, and thus are difficult to characterize with field instruments. Disturbances in the water can hinder settling or break up sediment flocs. Recognizing that each method has its own advantages and disadvantages, we estimated settling velocity using three independent methods. First, we used the eddy covariance method, based on a 200-day time series at a single location. Second, we used floc cameras, which provide the most accurate measurements of particle size that can be related to settling velocity, but lack temporal resolution. Third, we used the Rouse profile inversion, from data collected at fourteen different stations. The results are used to provide a robust assessment of mud settling velocity, and to provide guidance on the management of river diversions. A high floc settling velocity could be beneficial to a diversion project as higher settling will promote greater mass deposition and therefore land gain near the diversion as opposed to potentially advecting muddy sediment distally

from its source.

2. Methods

2.1. Study site

Barataria Basin is a large and shallow (~2 m deep) deltaic estuary located between the Mississippi River and a historical channel of the Mississippi River (Bayou Lafourche). The upper portion of the basin is dominated by freshwater lakes and wetlands, and transitions to intermediate/brackish marshes before giving way to salt marshes that dominate adjacent to the nearshore interface, where a chain of barrier islands separate Barataria Bay from the Gulf of Mexico (Fig. 1). For centuries Barataria Basin was supplied freshwater and sediment via flooding from the Mississippi River, however extensive leveeing of the channel has restricted movement of materials and thus depleted of sediment and nutrient movement. As a consequence, Barataria Basin has undergone extensive land loss over the last ~100 years (Couvillion et al., 2016). Additional factors contributing to this include subsidence and eustatic sea-level rise, which combine to generate enhanced relative sea-level rise. Currently, freshwater is predominately supplied from the Davis Pond Freshwater Diversion, the Gulf Intracoastal Waterway (GIWW), and small siphons in the Mississippi River (Fig. 1; Mariotti et al., 2022).

Hydrodynamics within the Barataria Basin are complex and impacted by numerous factors. Small astronomical tides, ~0.4 m at the

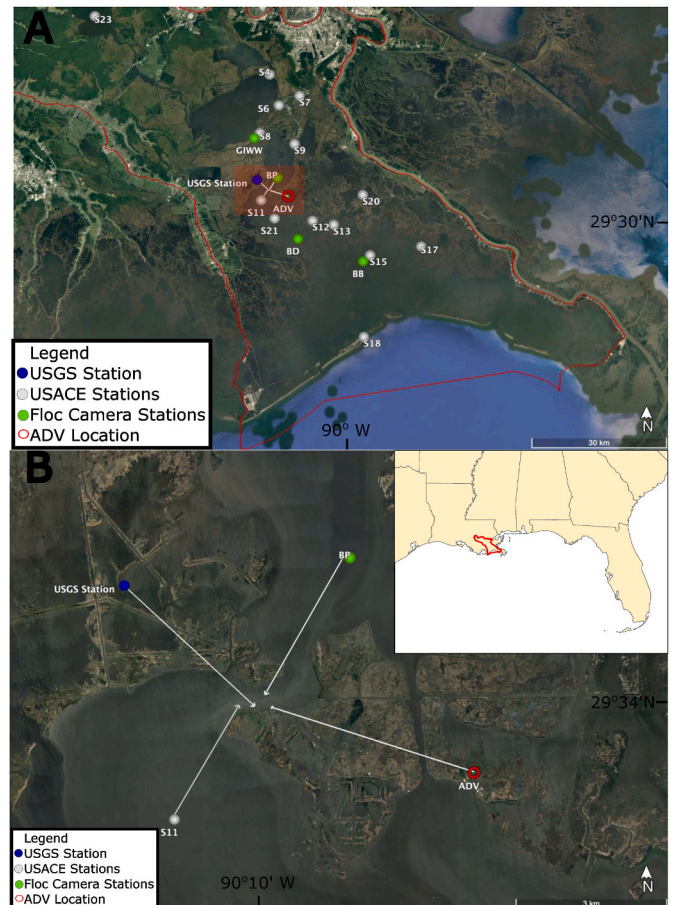


Fig. 1. Barataria Basin and site locations: The green dots are the floc camera stations, grey dots are USACE measurement sites, and blue dot is the USGS location, and red circle is the ADV location. The red outline indicates the extent of the Barataria Basin within the Northern Gulf of Mexico. Base map is provided by Google Earth. The red square in panel A is represented in panel B.

barrier inlets, dissipate landward (FitzGerald et al., 2007), and meteorological events, including tropical storms (summer-autumn months) and cold fronts (autumn-spring months) strongly affect water movement in southeast Louisiana. For example, following the passage of a cold front, greater than 40% of the estuary water volume can be flushed out in a two-day period (Feng and Li, 2010). While wind forcing is important for Barataria Basin hydrology, wave activity influenced by regional or remote wind activity plays a role in driving water exchange between the estuary mouth and nearshore region by driving current exchange across barrier inlets (Payandeh et al., 2019).

Salinity within Barataria Basin can vary drastically depending on the location. At Barataria pass (southern inlet) salinity can be relatively high (>21 psu); towards the center of the basin (Bayou Perot), salinity is very low (<1 psu); and near the basin head is fresh, i.e., 0 psu; Turner et al. (2019). Additionally, salinity is temporally conditioned by water discharge from the Mississippi River: it is well-documented that freshwater plumes from the Mississippi River can be advected through the barrier channels into the basin, thereby “freshening” the southern end of Barataria Bay (Walker et al., 2005).

2.2. Time-series measurements

2.2.1. Hydrodynamics

A 6000 kHz Acoustic Doppler Velocimeter (ADV) was deployed near the middle of Barataria Basin (90.16°N, 29.56°W) from November 5th, 2020, to May 24th, 2021. The three-dimensional velocity components ($\tilde{u}, \tilde{v}, \tilde{w}$) were measured hourly, 0.4 m above the bed, with a burst of 8192 points at 64 Hz. The velocity components were rotated so that the \tilde{u} was aligned with the principal channel direction. For each burst, the velocity, \tilde{u} , is decomposed into a mean, u , and a fluctuating velocity, u' (e.g., $\tilde{u} = u + u'$).

The bed shear stress produced by the water current was computed using three different techniques (Kim et al., 2000; Stapleton and Huntley, 1995). First, the bed shear stress was computed based on the turbulent kinetic energy (TKE),

$$TKE = (\overline{u'u'} + \overline{v'v'} + \overline{w'w'}) / 2. \quad (\text{Eq. 1})$$

To minimize the contamination from wave motion – which is irrotational rather than turbulent – the TKE was approximated by considering only the vertical velocity component (Stapleton and Huntley, 1995). Then, the resulting bed shear stress is

$$\tau_{TKE} = \rho 0.9 \overline{w'w'}, \quad (\text{Eq. 2})$$

where ρ is the water density (assumed to be 1000 kg/m³). Even with this method, however, the bed shear stress can still be affected by wave motion. Therefore, the values were discarded when the wave height was measured larger than 0.1 m.

Second, the bed shear stress was estimated from the depth-averaged velocity,

$$\tau_U = \rho C_D U^2, \quad (\text{Eq. 3})$$

where U is the depth-averaged mean velocity, which is set equal to 1.1 u , assuming a logarithmic profile, a water depth of 2 m, and a bed roughness z_0 equal to 1 mm. The drag coefficient C_D was calibrated by comparison with the τ_{TKE} (when the wave height was smaller than 0.1 m) and found equal to 0.0019.

Third, the bed shear stress was estimated from the TKE dissipation rate ϵ , which was calculated as

$$\epsilon = \frac{2\pi}{u} \frac{1}{f_2 - f_1} \int_{f_1}^{f_2} \left(\frac{\Phi(f) f^{5/3}}{\alpha} \right)^{3/2} df \quad (\text{Eq. 4})$$

where $\Phi(f)$ is the variance spectrum of the vertical velocity, and f_1 and f_2 are the limits of the inertial range of the spectrum, taken equal to 1 and 5

Hz. The value was discarded if the slope of the spectrum in this range is more than 50% different than the theoretical value of $-5/3$. The value α was set equal to 0.67 (Jabbari et al., 2020). Then, the bed shear stress is computed as

$$\tau_e = \rho \left[(kz\epsilon)^{1/3} \right]^2 \quad (\text{Eq. 5})$$

where k is the von Karman constant, equal to 0.4. For reference, we also calculate the shear dissipation rate G ,

$$G = \sqrt{\epsilon/\nu} \quad (\text{Eq. 6})$$

The significant wave height and peak period were calculated from pressure measurements at the bed using the standard linear wave theory (Wiberg and Sherwood, 2008). The wave bed shear stress was then estimated as

$$\tau_w = 0.5 \rho f_w U_b^2 \quad (\text{Eq. 7})$$

where U_b is the maximum bed orbital velocity associated with the significant wave height, and f_w is a bed friction coefficient, set equal to 0.015 (Collins, 1972).

2.2.2. Sediment dynamics

The acoustic backscatter of the ADV was used as a proxy for the total suspended sediment (TSS) using a previously proposed formula (Salehi and Strom, 2011),

$$TSS = 10^{(aS+b)}, \quad (\text{Eq. 8})$$

where S is the signal-to-noise ratio [dB] averaged for the three beams. The coefficients a and b were established through a laboratory calibration (Fig. 2), whereby preliminary experiments demonstrated that glass tanks were creating an unrealistic noise background, necessitating that calibration experiments be performed in a 2-m long, 1-m wide, and 40-cm deep plastic pool, locating the ADV head in a corner of the pool, facing inward.

In the experiment, we used tap water and sediment collected from the flank of a channel near the deployment site. The calibration experiment started with no sediment in the pool to establish a baseline measurement. From this point, known amounts of sediment were added in logarithmic increments beginning at 2 mg/l and finishing at 640 mg/l. A propeller was used to keep the water in constant motion and thus

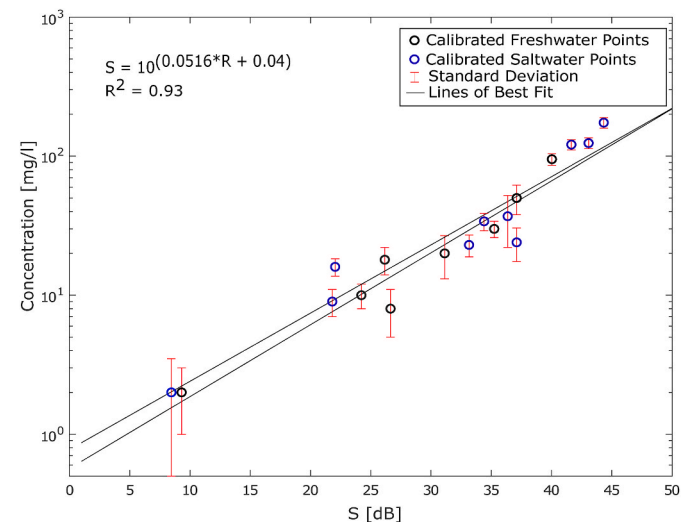


Fig. 2. Calibration curve of Total Suspended Sediments (TSS) vs. Signal to noise ratio (S). Considers salt (1 ppt) and freshwater trials and includes the standard deviation of each trial. Standard deviation represents the variation in concentration among the three different 1-L samples collected at each interval.

homogenize the sediment mixture. At each increment of sediment addition, a 3-min time series was collected by the ADV, and three 1-L water samples were collected 3 cm from the ADV using a siphon. The concentration value was calculated from the average of the three samples collected during each 3-min time series. The samples were filtered through 1 μ m glass fiber filters, then dried in an oven at 100 °C for 24 h. The difference between the filter pre-weight and post-weight was used to compute the TSS concentration for each increment. The calibration procedure was then repeated at the same logarithmic concentration levels (2 mg/l to 640 mg/l), but with added salt (1 ppt); however, no significant difference was determined when adding salt.

2.2.3. Settling velocity from eddy covariance

The vertical sediment flux was calculated from the covariance (Fugate and Friedrichs, 2002),

$$E = \overline{w'S'} \quad (\text{Eq. 9})$$

where S' is the instantaneous TSS, which is measured at 64 Hz as for the velocity.

Then, assuming that the suspended sediment concentration is in a steady state and spatially uniform (in the horizontal direction), the sediment deposition flux was set equal to the erosion flux. Assuming that the deposition flux is linearly related to the mean suspended sediment concentration ($S = \overline{S}$) through a constant settling velocity, the settling velocity w_s was calculated as:

$$w_s = \frac{\overline{w'S'}}{S} \quad (\text{Eq. 10})$$

Because this estimate of the settling velocity assumes that the suspended sediment concentration is in equilibrium with the local resuspension, it was only calculated when this condition was met. In practice this occurred during ebb currents but not during flood currents (see section 3.2).

2.2.4. Salinity and river discharge

Salinity was measured at a nearby USGS monitoring station (Bayou Perot at Point Legard, Fig. 1), located about 50 m from the ADV site. The USGS station also recorded turbidity, which has been previously calibrated to TSS (Mariotti et al., 2022). The turbidity data were only available from day 0 to day 22, and from day 110 to day 150.

Mississippi River discharge was retrieved from a USGS station located at Baton Rouge. This discharge was used as a proxy for the discharge into the GIWW (Swarzenski, 2003; Swarzenski and Perrien, 2015; Mariotti et al., 2022). As mentioned, while salinity in Barataria Bay varies spatially and temporally, it fluctuates greatly depending on the Mississippi River discharge (Ou et al., 2020).

2.3. Floc measurements

2.3.1. Floc camera measurements

In situ floc size measurements were made at four locations within the study region on January 13, 2021, from an 8-m survey vessel using the FlocARAZI imaging system paired with a CTD (Osborn et al., 2021). The FlocARAZI consists of a camera, microscope lens, and LED light source situated within a waterproof housing. The camera system has a field of view of 3.7 \times 2.8 mm and can resolve particles down to six microns in diameter. The system is designed to collect images while either profiling over the water column or when holding depth during deployment. At all times, a live video feed of imaged flocs is viewable by an onboard computer. Camera and light settings can be adjusted in real-time, as may be necessary. Images were collected over the depth of the water column at North Barataria Bay, in Bay Dosgris, at the ADV Perot station, and within the GIWW. Images of the suspended matter were collected at 2 Hz continuously over the profile, but the camera was set to collect images for multiple minutes at specific depth locations, holding the camera in

the vertical position, to ensure reliable size distribution statistics of imaged particles.

Measurements of particle area (based on pixel size) for each image were extracted using an automated, but tuned, particle extraction routine, similar to those outlined in Osborn et al. (2021). Two updates to the Osborn et al. method used to process the data included running the standard particle identification routines on differenced images only (a procedure that removed particles that show up in sequential images) and using an updated method to exclude out-of-focus particles from analysis. Measured particle areas were classified into groups based on water depth at each hold location during the profiling that included: surface, mid-depth, and bottom. The area of each particle was then converted to a physical length using the pixel-to-physical-length conversion factor (0.925 μ m/pixel) and then taking the effective floc diameter to be $d_f = \sqrt{4A/\pi}$. The volume associated with each measured particle or floc was then calculated as $V_f = \pi d_f^3/6$. The floc diameter, d_f , and volume, V_f , were used to develop volume-based particle-size distributions, which allowed the calculation particle-size distribution statistics.

2.3.2. Settling velocity from floc size

The settling velocity of any individual floc of size d_f was calculated using the settling velocity equation of (Strom and Keyvani, 2011):

$$w_s = \frac{gR_s d_f^{\eta_f - 1}}{b_1 \nu d_p^{\eta_f - 3} + b_2 \sqrt{gR_s d_f^{\eta_f} d_p^{\eta_f - 3}}} \quad (\text{Eq. 11})$$

where g is the acceleration of gravity, R_s is the submerged specific gravity of the primary particles ($R_s = (\rho_s - \rho)/\rho$ with ρ_s equal to the density of the primary particles and ρ equal to the fluid density), η_f is the floc fractal dimension, d_p is the diameter of the primary particles of which the floc is composed, ν is the kinematic viscosity of the fluid, and b_1 and b_2 are model coefficients related to the floc shape and porosity. Eq. (11) provides an estimate of the settling velocity for a measured floc size, d_f , given input values for ρ , ν , d_p , ρ_s , η_f , b_1 , and b_2 .

Strom and Keyvani (2011) provide a full sensitivity analysis of the model based on changes in d_p , ρ_s , η_f , b_1 , and b_2 , and compare and calibrate the model to paired floc size and settling velocity data. Based on their analysis and recommendations, we used $\eta_f = 2.5$, $d_p = 5 \mu$ m, $\rho_s = 2500 \text{ kg/m}^3$, and model coefficients $b_1 = 120$ and $b_2 = 0$ as reasonable first-pass values for estimation of settling velocity. These model parameter values have also been shown to be reasonable values to use when predicting settling velocity using floc size (Markussen and Andersen, 2013; Osborn et al., 2023). Fluid density and viscosity were set using the temperature and salinity measured with the CTD during profiling.

A distribution average settling velocity was also calculated for each hold location in the vertical at each of the four stations. The distribution average settling velocity, w_s , at each hold location was calculated using the fraction of material in each size class by volume, f_i , and the log centered size associated with each class, d_i . For each d_i , the associated settling velocity, w_{si} , was calculated using the Strom and Keyvani (2011) equation as previously described. The distribution average settling velocity was then obtained by summing the product of the size-class settling velocity with the fraction of material in that size class, $w_s = \sum_{i=1}^n f_i w_{si}$, where n is the total number of size classes in each distribution.

2.4. Basin-wide TSS survey

2.4.1. Data collection

Beginning in January 1997, the U.S. Army Corps of Engineers (USACE) began sampling a transect of stations throughout Barataria Basin. In total, 23 stations were sampled at certain times once a month

until 2006. Different parameters were measured at the top and bottom of the water column, including salinity, turbidity, pH, and temperature. Not every station has a complete set of data, so those stations without full data were omitted from further analysis, yielding 14 stations total.

2.4.2. Settling velocity from Rouse profile inversion

A third method used to estimate w_s relies on the inversion of a Rouse sediment concentration profile, which is one of the first works regarding the balance of settling and turbulence (i.e., Rouse, 1937). This model is well-documented for subaqueous sediment-laden flows (e.g., Boudreau and Hill, 2020; de Leeuw et al., 2020), whereby the equation is based on the assumption that the upward flux of sediment via turbulence is balanced by downward gravitational settling. The Rouse equation can be arranged in the following way:

$$R = \frac{-\log \frac{C_t}{C_b}}{\log \left[\frac{z_m}{(h-z_m)} \frac{h-z_o}{z_o} \right]}, \quad (\text{Eq. 12})$$

where C_t is TSS (mg/l) measured at the top of the water column, C_b is the TSS at the bottom of the water column, z_b is the elevation above the bed at which the bottom TSS (C_b) is measured (which was assumed to be 0.1 m), z_m is the depth below the water surface where the surface layer is measured (estimated here to be 0.2 m), and h is the water depth at each individual sampling location. Across the 14 stations, h varied from 1.0 m to 5.4 m (where the deepest measurement is at the channel inlet in Grand Isle). After calculating the Rouse number (R) the settling velocity is calculated as:

$$w_s = R\kappa\sqrt{\tau/\rho}, \quad (\text{Eq. 13})$$

whereby τ is the bed shear, which was estimated to be equal to 0.4 Pa, an assumption that is discussed later.

3. Results

3.1. Hydrodynamics

The magnitude of the depth-average, along-channel velocity (U) ranged from 0 to 0.8 m/s (Fig. 3). During the entirety of the deployment, there was a net seaward velocity of 0.13 m/s. Water levels and velocity

fluctuations were associated with both astronomical and meteorological tides. Abrupt reversals of U were associated with the approach and passage of cold fronts, during which the wind first blows from the southeast, and then abruptly reverts to blow from the north (Payandeh et al., 2019). Cold fronts were also associated with the highest wave heights, which were up to 0.55 m.

Higher salinity (5–10 psu) was recorded early in the deployment (November–December), in conjunction with a lower discharge from the Mississippi River, and hence also from the GIWW. At the end of the deployment (April–May) salinity was low (0–1 psu), in concomitance of a higher riverine discharge. The average salinity throughout the period was 1.2 psu. Salinity fluctuations were also associated with velocity fluctuations. Salinity increased when the flow was directed landward, and then decreased as northerly winds forced water out of the bay.

All three methods used to estimate current bed shear stress gave similar results. Through a single calibration of the drag coefficient, τ_U and τ_{TKE} had a high correlation ($R^2 = 0.88$) (Fig. 5). Overall, the bed shear stress was dominated by currents than by waves.

3.2. Sediment dynamics

The TSS calibration in the lab was robust ($R^2 = 0.93$) and showed no sensitivity with respect to water salinity. TSS estimated from the backscatter data aligns closely ($\pm 30\%$) with TSS estimated from the turbidity sensor, which was previously calibrated with independent data (Mariotti et al., 2022) (Fig. 2).

Two distinct TSS trends were identified: a slow changing baseline, and a fast changing series of spikes. The baseline increased from 30 to 40 mg/l during November and December (approximately days 0–30), to 60–70 mg/l during April and May (days 160–200). TSS also fluctuated with peaks of about 300–400 mg/l, which occurred in concomitance of high currents (Fig. 3).

During ebb, TSS was correlated with the bed shear stress, indicating that the sediment was locally resuspended. (Fig. 6). During flood, there was no correlation between shear stress and TSS, suggesting lateral advection of sediment.

3.3. Settling velocity from eddy covariance

Settling velocity estimated from eddy covariance varied from 0.1 to

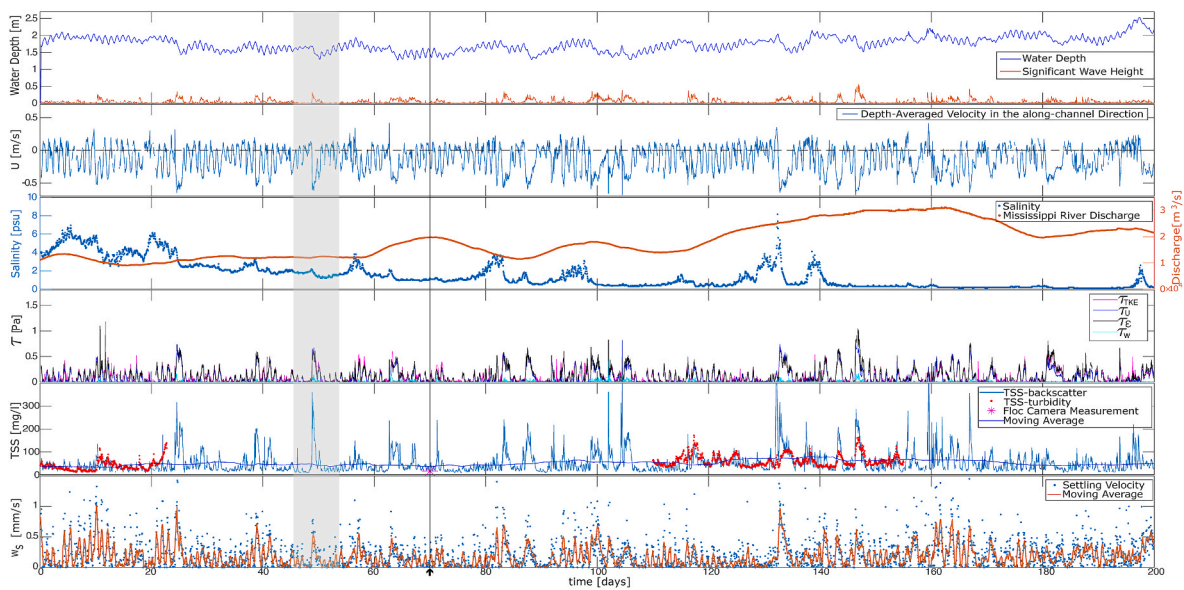


Fig. 3. Time series at the ADV locations, starting from 11/05/2020 and ending 5/24/2021. A negative U along-channel component is defined as leaving the bay, (southerly direction). The orange line in the bottom panel is the moving average, considering a window of 10 days. The grey, shaded box represents a cold front (Fig. 4), while the arrow points to the thin, blackline on the day in which floc camera measurements were taken.

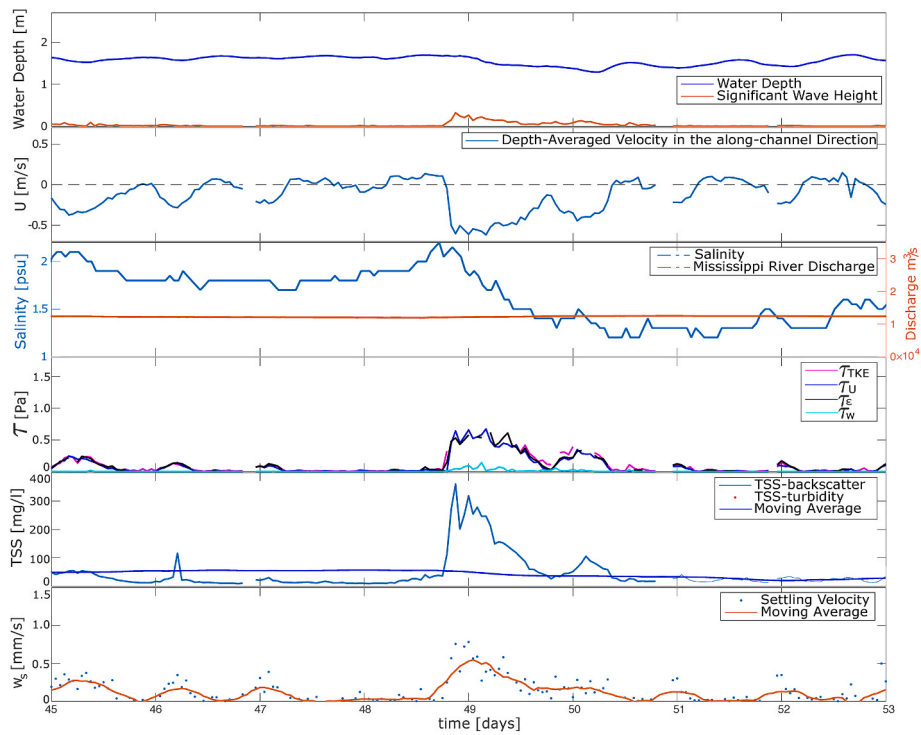


Fig. 4. Cold front passage during ADV deployment (shaded, grey box from Fig. 3).

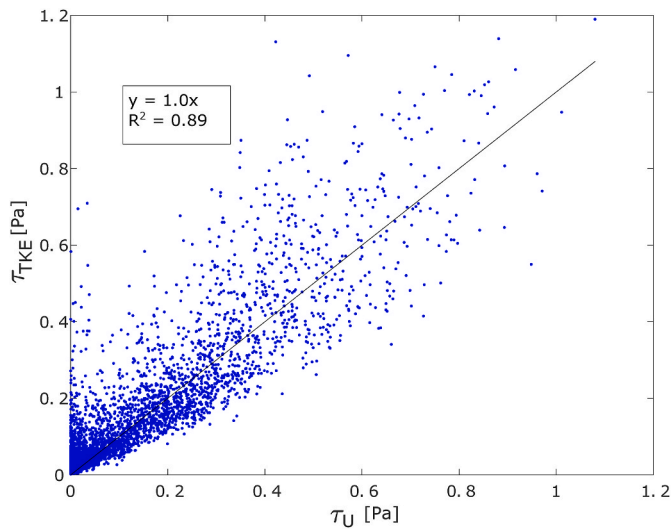


Fig. 5. τ_U vs τ_{TKE} . The solid line indicates the best linear fit. The slope of the curve is equal to one because these data were used to calibrate the drag coefficient in τ_U (Eq. (2)).

1.5 mm/s (Fig. 3). Settling velocity increased with turbulence, when quantified through either TKE, G , or τ_U (Fig. 7). For larger turbulent levels ($TKE > 0.0015 \text{ m}^2/\text{s}^2$, $G > 5 \text{ Hz}$, $\tau_U > 0.4 \text{ Pa}$), settling velocity remained relatively constant for a given salinity.

For the highest level of turbulence recorded ($G > 5 \text{ Hz}$), settling velocity increased with salinity. For example, for $G > 5 \text{ Hz}$, settling velocity was on average 0.8 mm/s for a salinity greater than 4 psu but only 0.4 mm/s for a salinity of 0–2 psu.

3.4. Floc measurements

Floc measurements at the four stations were taken during a period

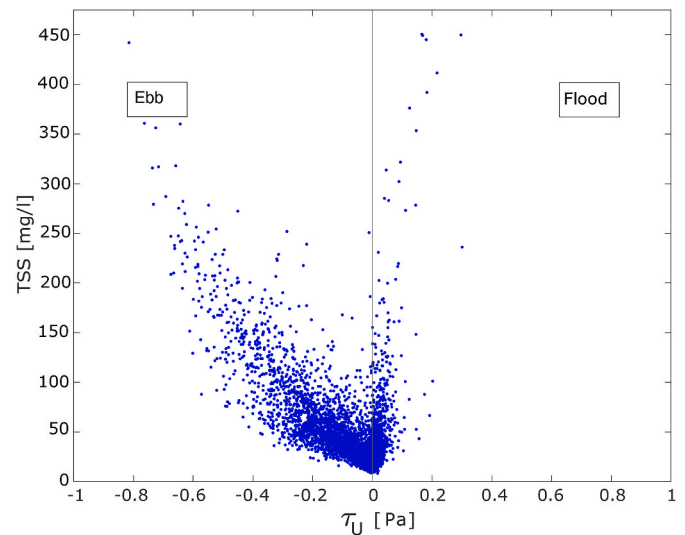


Fig. 6. TSS as a function of bed shear stress (τ_U), separated into flood (landward directed) and ebb (seaward directed).

with a moderate river discharge (20,000 m^3/s in the Mississippi River), when the flow was slow and directed seaward ($U \sim 0.2 \text{ m/s}$), and waves were small ($H_s = 0.01 \text{ m}$). Salinity ranged from 4 psu at the most seaward station to 0 psu at the most landward station. The bed shear stress at the ADV location, when the flocs were measured, was 0.2 Pa.

At three of the four stations (Bay Dosgrais, Barataria Bay, and Perot) floc size was slightly larger (20%) near the bottom than near the top of the water, indicating an equilibrium between resuspension from the bed and deposition from the water column (Fig. 8).

The floc size distribution was similar at all stations, with a d_{50} from 135 to 150 $\mu \text{ m}$, leading to a similar estimated settling velocity (0.3–0.5 mm/s) at all four stations (Fig. 8). The depth-averaged settling at the Perot site (where the ADV was located) estimated from the floc camera

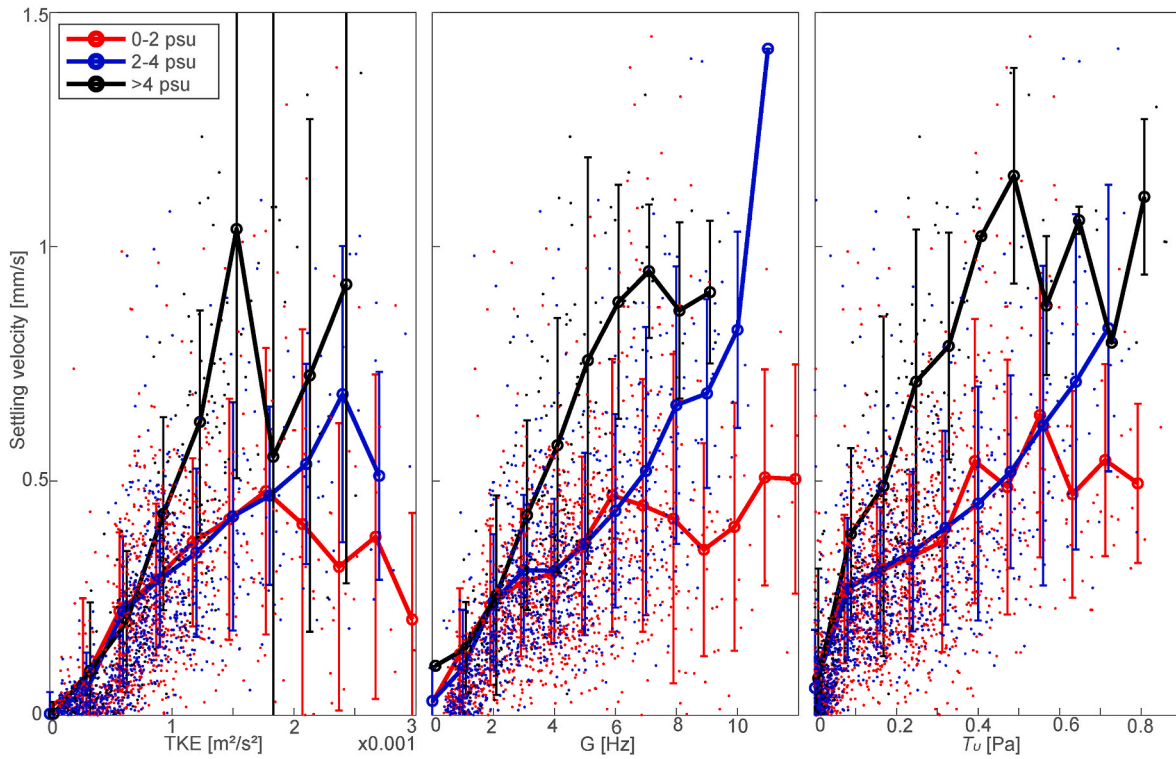


Fig. 7. Settling velocity as a function of turbulent kinetic energy (TKE), Shear rate (G), and current-induced bed shear stress (τ_U), for three different ranges of salinities. Values are only reported for ebb currents, for which the suspended sediment concentration is in equilibrium with local bed resuspension. Small dots are hourly values; large circles are binned means; errorbars are binned standard deviations.

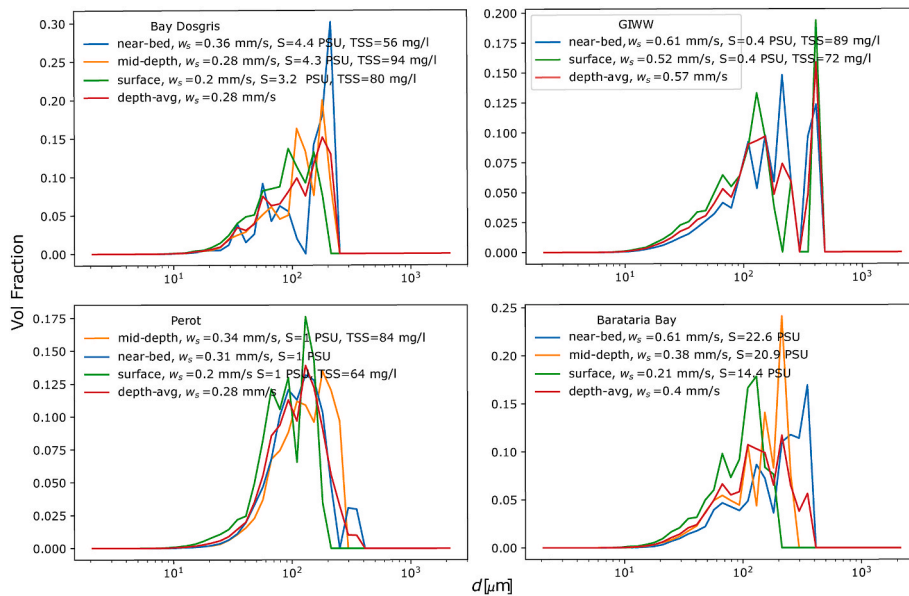


Fig. 8. Floc measurements. Floc size distribution at different depths and different locations (see Fig. 1).

was 0.28 mm/s (Fig. 3). The value estimated from the eddy covariance at that time was 0.29 mm/s (Fig. 3).

3.5. Basin-wide survey of TSS and Rouse profile inversion

Stratification has been shown to be a key driver of flocculation in certain salinity and turbulence regimes (Zhang et al., 2018). We considered the temperature and salinity data measured at the top and the bottom of the water column and found no evidence of vertical

stratification. Therefore, stratification is neglected when computing the settling velocity from the Rouse profile inversion.

Settling velocity derived from the basin-wide sampling ranged from 0 (when TSS was uniform in the vertical or slightly higher on the top than the bottom) to 1.5 mm/s, with a median value of 0.27 mm/s. No trend in settling velocity was detected when grouping the stations into three regions (lower, middle, and upper basin), nor when dividing it into different levels of salinity or TSS (Figs. 9 and 10).

The estimated settling velocity is accompanied with uncertainty,

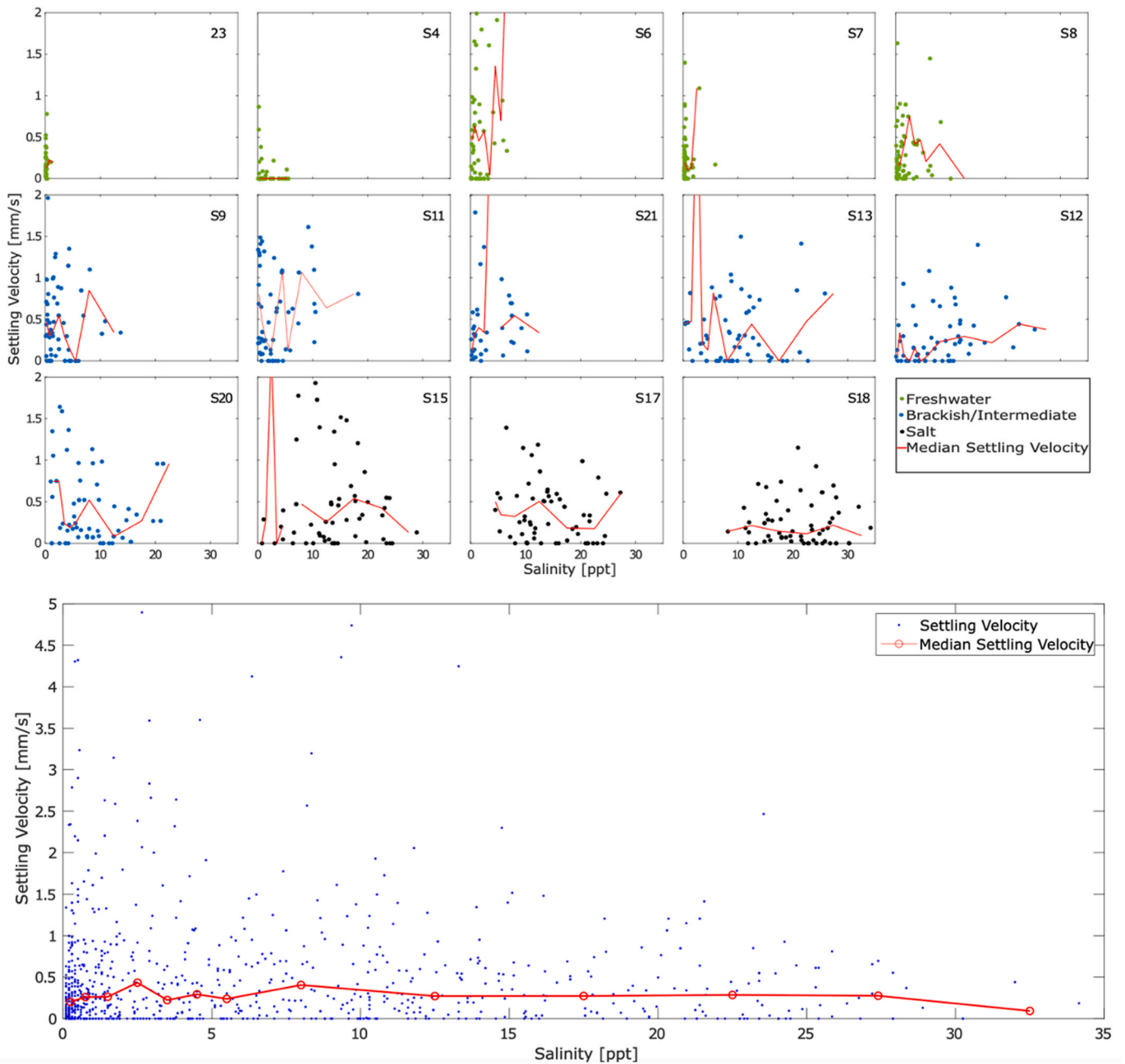


Fig. 9. Settling velocity estimated from the Rouse profile inversion at fourteen stations through Barataria Basin (Fig. 1), plotted as a function of salinity.

mainly from the assumption of a constant bed shear stress at all sites and at all times. We assumed a relatively low bed shear stress because, for logistical reasons, water samples were collected during fair weather conditions, i.e., when cold fronts and thus strong currents are not present. Also, assuming they were sampled randomly throughout the astronomical tidal cycle, they were more likely to be sampled during a period with low to absent currents than during peak flood or ebb currents. Considering the ADV location, for example, the 95th percentile of the τ_U is 0.33 Pa.

As a sensitivity test, we recalculated the settling velocity (Eq. (13)) using a different value for the bed shear stress, either smaller or larger than the reference value of 0.4 Pa. For a bed shear stress of 0.2 Pa, the settling velocity was 29% lower than the settling velocity calculated with the reference value, whereas for a bed shear stress of 0.8 Pa the settling velocity was 41% higher than the settling velocity calculated with the reference value. Thus, for a wide range of the assumed bed

shear stress, the settling velocity estimated from the Rouse profile inversion aligns closely with the settling velocity estimated with the eddy covariance and the floc-camera method. For example, the median settling velocity of 0.27 mm/s, obtained from a Rouse profile inversion, is similar to the mean value obtained from the eddy covariance method (0.20 mm/s) as well as from the floc camera (0.31 mm/s).

4. Discussion

4.1. Barataria Basin: a highly dynamic hydro-sedimentary environment

The hydrodynamics in Barataria Basin is regulated by river discharge and astro-meteorological currents. The latter is strongly controlled by cold fronts, which creates a strong ebb current (Li et al., 2021; Payandeh et al., 2019). The interplay between river discharge and astro-meteorological currents explains the salinity and sediment

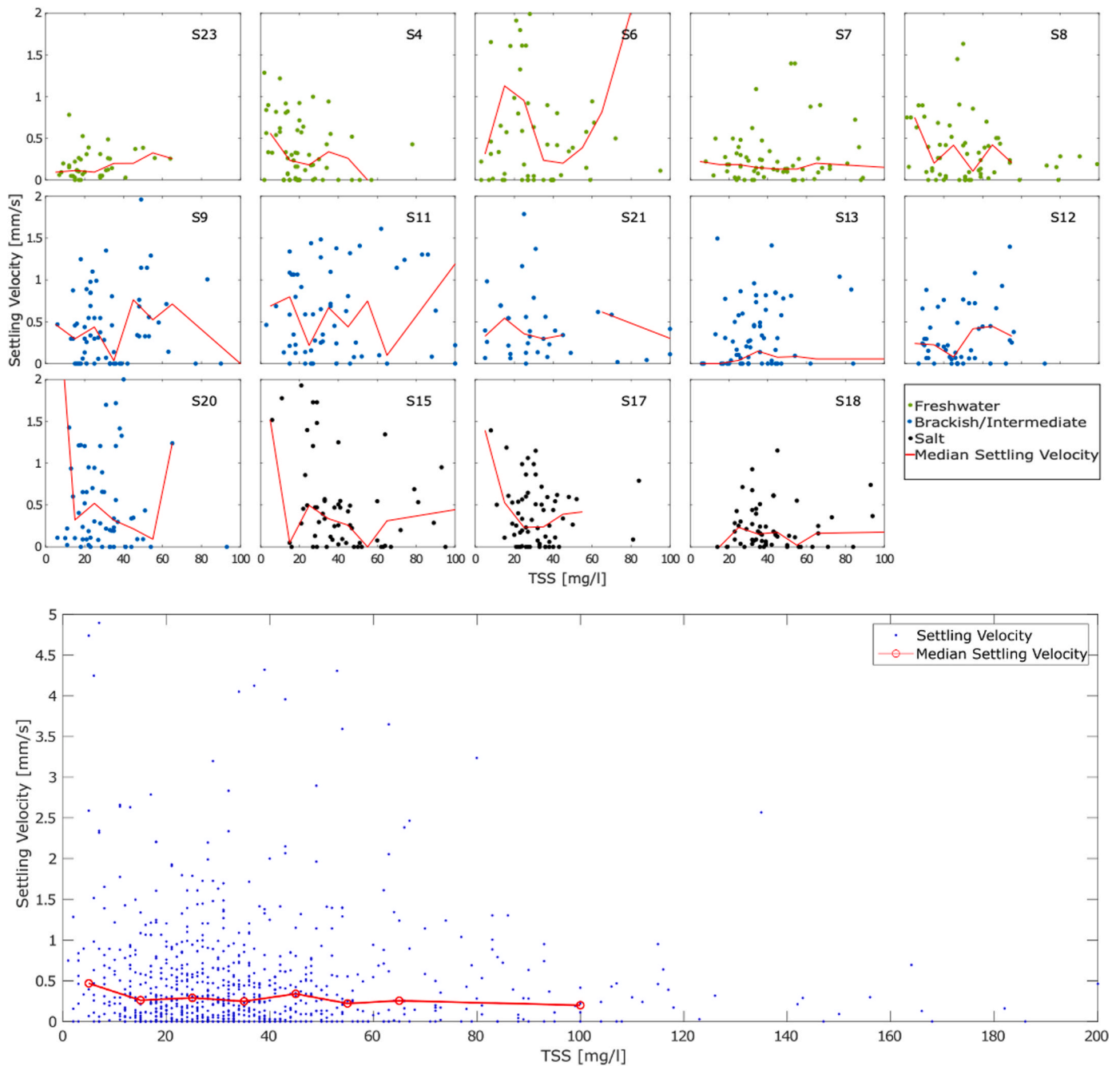


Fig. 10. Settling velocity estimated from the Rouse profile inversion at fourteen stations through Barataria Basin (Fig. 1), plotted as a function of TSS.

dynamics observed at the ADV location.

River discharge controls the slow varying response, i.e., the baseline values. Early in the deployment, when the river discharge was low, salinity was high and baseline TSS was low. As the discharge increased during the spring, freshwater and sediment were imported into Barataria basin through the GIWW (Mariotti et al., 2022), which then decreased salinity and increased the baseline TSS. The increase in the TSS baseline from 30 to 40 mg/l to 60–70 mg/l (Fig. 3) is consistent with previous estimates from long-term field monitoring and remote sensing in the same area (Mariotti et al., 2022).

Astro-meteorological currents control the quickly varying response, and especially the peak values, in TSS. These peaks were associated with either local sediment resuspension or lateral advection. Local resuspension by current flow is clearly observed during ebb currents, for which there is a strong correlation between bed shear stress and TSS

(Fig. 6). Lateral advection is most evident during flood currents when TSS is high despite small bed shear stress and hence negligible local resuspension at the ADV site (Fig. 6). These sediments are likely resuspended in lower Barataria Bay (which is more open and thus more prone to wave-induced resuspension) and then advected landward. The same advection also explains the temporary increase in salinity from 0 to ~5 psu during flood currents, as the saltier water from lower Barataria Bay is pushed landward (Ou et al., 2020).

The variability in salinity and currents (and hence turbulence regime) set the stage for variable flocculation dynamics. In particular, the variability in salinity and turbulence is larger than that present in previous studies of mud flocculation (Fugate and Friedrichs., 2002; Osborn et al., 2023), and hence provides the opportunity to develop robust predictions.

4.2. Turbulence and salinity regulate flocculation

Settling velocity at the ADV site increases monotonically with TKE , τ_U , and G (Fig. 7). This suggests that within this “lower turbulence regime”, the limiter on suspended floc size is the ability of turbulence to keep flocs or other particulates in suspension. Theoretical models predict that this regime is present for values of the shear rate G smaller than about 10–20 Hz (Kumar et al., 2010; Son and Hsu, 2008; Winterwerp et al., 2006b). Consistent with this finding, the shear rate measured at the ADV sites was always smaller than 10 Hz. For the lowest salinity (0–2 psu), settling velocity starts to decrease at a shear rate of about 8 Hz, suggesting a regime in which turbulence just starts to break up flocs.

In addition to turbulence, settling velocity increases with salinity, which is consistent with previous studies (Abolfazli and Strom, 2022; Al Ani et al., 1991; Mikeš and Manning, 2010). For example, for a shear rate of 5 Hz, the settling velocity is 0.4 mm/s with a salinity less than 2 psu. Conversely, at the same shear rate level, but with a salinity greater than 4 psu, the settling velocity increases to 0.8 mm/s. Notably, the salinity effect is absent at low levels of turbulence ($G < 5$ Hz). Indeed, in this regime, the floc size is not directly affected by its growth and destruction, but rather by the ability of the flow to keep flocs in suspension. Only when the flocculated sediment can be kept in suspension for a significant amount of time does salinity (which tends to increase the aggregation rate of the sediment) become a factor in determining the equilibrium size of the flocs.

The floc camera measurements in the GIWW provide clear evidence that mud is flocculated in freshwater (e.g., salinity < 0.4 psu). Notably, the measured floc size and the estimated settling velocity was similar at all sites, whose salinity ranged from 0.4 to 20 psu (Fig. 8). The observed flocculation in freshwater is likely enabled by the relatively higher organic content within the estuary and the background ion concentration. Mud particles can be strongly influenced by the different types of organic matter (OM) found in estuaries, enhancing flocculation (Furukawa et al., 2014; Mietta et al., 2009), as organic matter can “glue” flocs together (Eisma, 1986). Over a 22-year study near the observation site (Turner et al., 2019), the OM concentration of the suspended sediment was shown to be over 25%. This is much higher than the nearby Mississippi River, where OM concentration has been documented to have lower values than Barataria Basin (Waterson and Canuel, 2008) – about 3% – but yet enough to sustain freshwater flocculation (Osborn et al., 2023).

Contrary to the results obtained by the eddy covariance method, settling velocity estimated from the Rouse profile inversion did not have a clear dependence on salinity. We speculate that this occurs for two reasons. First, the measurements were taken during low levels of turbulence (e.g., $G < 5$ Hz), for which the eddy covariance method suggests that there is no dependence on salinity. Second, even when the measurements were taken in the regime where salinity should have an effect, uncertainty about the level of turbulence prevents us from identifying the influence of salinity – i.e., the noise is larger than the signal.

We also noticed that TSS did not have an effect on settling velocity, as has been found in other estuaries. Indeed, mud settling velocity has often been positively correlated with TSS (Winterwerp, 1998; Winterwerp et al., 2006b; Whitehouse et al., 2000), especially for TSS greater than 1000 mg/l. The absence of a TSS effect at our site likely occurs because the range of the observed TSS in mid-Barataria Bay is relatively small, i.e., between 10 and 500 mg/l.

4.3. Implications for sediment diversions and modeling sediment transport dynamics

The three independent methods for estimating settling velocity provide consistent results and thus provide a robust input to inform mud dynamics in Barataria Basin. In particular, the relationship among settling velocity, turbulence, and salinity to floc size and settling velocity can better constrain parameters that have been used in numerical

models of Barataria Basin. For example, a settling velocity of 0.001 mm/s, assigned to unflocculated clay particles in Barataria Basin (Baustian et al., 2018) is not realistic. Even in freshwater, mud settling velocity is at least 0.1 mm/s for any appreciable level of turbulence (e.g., $\tau_U > 0.01$ Pa) due to the flocculated nature of the sediment. A settling velocity of 0.1 mm/s assumed in a different study (Zang et al., 2019) is, therefore, a more realistic value; nonetheless, we argue that a value of 0.1 mm/s likely remains an underestimate, as all methods herein show that average settling velocity is 0.2–0.3 mm/s.

Changes in settling velocity fundamentally alter predictions of where mud accumulates. Settling velocity, therefore, affects the outcome of models that seek to evaluate land loss and gain in this dynamic environment. Prior model simulations indicate that orders of magnitude changes in settling velocity greatly impact how far mud delivered by the river is dispersed before accumulating in coastal Louisiana (Xu et al., 2016). With respect to the planned river diversion in Barataria Basin, too low of a settling velocity would predict mud entirely exiting the basin. Alternatively, too high of a settling velocity would predict mud accumulation very close to the diversion outlet. In all, incorrect settling velocity values used in models predicting wetland gain and/or loss will lead to projections different than reality.

At the ADV site, in middle Barataria Basin, mud settling velocity increased monotonically with turbulence, indicating that flocs and other particulates are resuspension-limited rather than growth limited. Similar levels of turbulence are likely found in most other areas of Barataria Basin. Hence, we suggest that floc dynamics throughout Barataria Basin is transport limited, and thus the areas with relatively higher turbulence (e.g., where currents are on the order of 0.5 m/s) should experience higher settling velocity than the areas with lower turbulence (e.g., sheltered areas with slow currents).

A different dynamic is present in the nearby main channel of the Mississippi River, where turbulence is high enough to limit floc size in some regions of the river. Field measurements with a floc camera show indeed that floc size increases progressing from the Bonnet Carré Spillway to Venice, in association with a decrease in flow speed and turbulence (Osborn et al., 2023). Similar or greater turbulence will likely be found at the outlet of an engineered river diversion, as that planned for Barataria Basin (Xu et al., 2016). These energetic conditions could break flocs apart and decrease mud settling velocity, thus decreasing the ability to trap this mud. However, in the far-field of the diversion, it is likely that bed shear stress would be less than 1 Pa (i.e., currents smaller than ~ 0.8 m/s) (Fig. 3); that is, values similar to those typically found in Barataria Basin. Under such turbulence regimes, it is likely that flocs sizes would increase rapidly enough to allow for mud entering the basin via the diversion to settle and be retained.

4.4. Future work

A crucial question concerns the fate of the mud as it reaches the vegetated marshes of Barataria Basin. There the velocity is generally low, on the order of 0.1 m/s and most likely less than 0.5 mm/s (Friedrichs and Perry, 2001). Based on the bed-generated turbulence, the flocs should be in the transport limited regime and thus should decrease in size with a decrease in turbulence within the suspension as larger material settles. On the other hand, turbulence could also be generated by the interaction between the flow and the vegetation, and thus might be much larger than that generated by bed friction (Nepf, 2012). Furthermore, the direct interaction between the flocs and the vegetation, e.g., interception by stems and leaves (Stein et al., 2021), could affect the transport characteristics of the flocs.

Another unresolved question concerns the flocculation state during extreme events such as hurricanes. During these events the turbulence levels in Barataria Basin might become large enough to induce floc breaking and reduce its settling velocity, potentially increasing the loss of mud toward the open ocean. Also, the suspended sediment concentration might reach levels high enough to hinder settling (Whitehouse

et al., 2000), a condition that was not observed during our deployment.

5. Conclusions

Mud settling velocity in Barataria Basin was estimated using three independent field methods. The three methods provide consistent results, demonstrate that mud is flocculated for salty, brackish, and freshwater conditions in Barataria Basin, and indicate that the size of floccules is dependent on both turbidity and salinity.

Throughout Barataria Basin, mud settling velocity measures 0.2–0.5 mm/s, which ranges from two orders of magnitude to a factor of three higher than previous estimates. As such, previous model predictions have likely underestimated the ability of mud to be retained within Barataria Basin.

In middle Barataria Basin, mud settling velocity increases monotonically with turbulence, presumably never reaching a regime where high turbulence levels limit floc size. This is likely due to the relatively low energy of the estuary even during cold fronts. This regime differs from that encountered in the Mississippi River, where turbulence can be high enough in some locations to limit floc sizes.

Consistent with other measurements in the Mississippi River, mud is flocculated in freshwater, likely because of the high organic content and relatively high background ion concentration for freshwater. This implies that the mud delivered by an engineered river diversion (which carries fresh water) has the potential to flocculate and to have a relatively high settling velocity. In this study, salinity was found to be correlated with an increase in settling velocity of up to a factor two, especially at the transition between 0 and 5 psu. Hence, an increase in mud deposition might occur at the transition between fresh and brackish water within Barataria Basin.

CRediT authorship contribution statement

M. McDonell: Formal analysis, Investigation, Writing – original draft. **K. Strom:** Formal analysis, Investigation, Writing – review & editing. **J. Nittrouer:** Investigation, Resources, Writing – review & editing. **G. Mariotti:** Conceptualization, Investigation, Methodology, Project administration, Supervision, Writing – review & editing.

Declaration of competing interest

The authors declare that we have no interests to disclose.

Data availability

Data will be made available on request.

Acknowledgements

This work was partially supported by the Louisiana Coastal Protection and Restoration Authority and the Louisiana Sea Grant, through an assistantship (Coastal Science Assistantship Program) to M.M. This work was partially supported by the National Science Foundation grant under EAR award 1801118, to JAN and KS.

References

- Abolfazli, E., Strom, K., 2023. Salinity impacts on floc size and growth rate with and without natural organic matter. *J. Geophys. Res.: Oceans* 128 (7) e2022JC019255.
- Abolfazli, E., Strom, K., 2022. Deicing Road salts may Contribute to Impairment of Streambeds through Alterations to Sedimentation processes. *ACS EST Water* 2, 148–155. <https://doi.org/10.1021/acestwater.1c00300>.
- Al Ani, S., Dyer, K.R., Huntley, D.A., 1991. Measurement of the influence of salinity on floc density and strength. *Geo Mar. Lett.* 11, 154–158. <https://doi.org/10.1007/BF02431002>.
- Baustian, M.M., Meselhe, E., Jung, H., Sadid, K., Duke-Sylvester, S.M., Visser, J.M., Allison, M.A., Moss, L.C., Ramatchandirane, C., Sebastiaan van Maren, D., Jeuken, M., Bargu, S., 2018. Development of an Integrated Biophysical Model to represent morphological and ecological processes in a changing deltaic and coastal ecosystem. *Environ. Model. Software* 109, 402–419. <https://doi.org/10.1016/j.envsoft.2018.05.019>.
- Boudreau, B.P., Hill, P.S., 2020. Rouse revisited: the bottom boundary condition for suspended sediment profiles. *Mar. Geol.* 419, 106066 <https://doi.org/10.1016/j.margeo.2019.106066>.
- Collins, J.I., 1972. Prediction of shallow-water spectra. *J. Geophys. Res.* 77, 2693–2707. <https://doi.org/10.1029/JC077i015p02693>.
- Couvillion, B.R., Fischer, M.R., Beck, H.J., Sleavin, W.J., 2016. Spatial Configuration trends in coastal Louisiana from 1985 to 2010. *Wetlands* 36, 347–359. <https://doi.org/10.1007/s13157-016-0744-9>.
- CPRA, 2017. Louisiana's Comprehensive Master Plan for a Sustainable Coast. CPRA. Draft Plan Release, Baton Rouge, Louisiana.
- de Leeuw, J., Lamb, M.P., Parker, G., Moodie, A.J., Hought, D., Venditti, J.G., Nittrouer, J.A., 2020. Entrainment and suspension of sand and gravel. *Earth Surf. Dyn.* 8, 485–504. <https://doi.org/10.5194/esurf-8-485-2020>.
- Droppo, I.G., Jeffries, D.S., Jaskot, C., Backus, S.M., 1998. The prevalence of freshwater flocculation in cold regions: a case study from the mackenzie river delta, Northwest Territories, Canada. *Arctic* 51, 155–164. <https://doi.org/10.14430/arctic1056>.
- Eisma, D., 1986. Flocculation and de-flocculation of suspended matter in estuaries. *Neth. J. Sea Res.* 20, 183–199. [https://doi.org/10.1016/0077-7579\(86\)90041-4](https://doi.org/10.1016/0077-7579(86)90041-4).
- Feng, Z., Li, C., 2010. Cold-front-induced flushing of the Louisiana bays. *J. Mar. Syst.* 82, 252–264. <https://doi.org/10.1016/j.jmarsys.2010.05.015>.
- FitzGerald, D., Kulp, M., Hughes, Z., Georgiou, I., Miner, M., Penland, S., Howes, N., 2007. Impacts of rising sea level to backbarrier wetlands, tidal inlets, and barrier islands: Barataria coast, Louisiana. In: Coastal Sediments '07. Presented at the Sixth International Symposium on Coastal Engineering and Science of Coastal Sediment Process. American Society of Civil Engineers, New Orleans, Louisiana, United States, pp. 1179–1192. [https://doi.org/10.1061/40926\(239\)91](https://doi.org/10.1061/40926(239)91).
- Fox, J., Ford, W., Strom, K., Villarini, G., Meehan, M., 2014. Benthic control upon the morphology of transported fine sediments in a low-gradient stream: benthic control on transported sediment morphology. *Hydrol. Process.* 28, 3776–3788. <https://doi.org/10.1002/hyp.9928>.
- Friedrichs, C.T., Perry, J.E., 2001. Tidal Salt Marsh Morphodynamics: A Synthesis. *J. Coastal Res.* SI 27, 7–37.
- Fugate, D.C., Friedrichs, C.T., 2002. Determining concentration and fall velocity of estuarine particle populations using ADV, OBS and LISST. *Continental Shelf Res.* 22, 1867–1886. [https://doi.org/10.1016/S0278-4343\(02\)00043-2](https://doi.org/10.1016/S0278-4343(02)00043-2).
- Furukawa, Y., Reed, A.H., Zhang, G., 2014. Effect of organic matter on estuarine flocculation: a laboratory study using montmorillonite, humic acid, xanthan gum, guar gum and natural estuarine flocs. *Geochem. Trans.* 15, 1. <https://doi.org/10.1186/1467-4866-15-1>.
- Izquierdo-Ayala, K., Garcia-Aragon, J.A., Castillo-Uzcanga, M.M., Salinas-Tapia, H., 2021. Freshwater flocculation dependence on turbulence properties in the usumacinta river. *J. Hydraul. Eng.* 147, 05021009 [https://doi.org/10.1061/\(ASCE\)HY.1943-7900.0001940](https://doi.org/10.1061/(ASCE)HY.1943-7900.0001940).
- Jabbari, A., Boegman, L., Valipour, R., Wain, D., Bouffard, D., 2020. Dissipation of turbulent kinetic energy in the oscillating bottom boundary layer of a large shallow lake. *J. Atmos. Ocean. Technol.* 37, 517–531. <https://doi.org/10.1175/JTECH-D-19-0083.1>.
- Kim, S.-C., Friedrichs, C.T., Maa, J.P.-Y., Wright, L.D., 2000. Estimating bottom stress in tidal boundary layer from acoustic Doppler velocimeter data. *J. Hydraul. Eng.* 126, 399–406. [https://doi.org/10.1061/\(ASCE\)0733-9429\(2000\)126:6\(399\)](https://doi.org/10.1061/(ASCE)0733-9429(2000)126:6(399)).
- Kumar, R.G., Strom, K.B., Keyvani, A., 2010. Floc properties and settling velocity of San Jacinto estuary mud under variable shear and salinity conditions. *Continental Shelf Res.* 30, 2067–2081. <https://doi.org/10.1016/j.csr.2010.10.006>.
- Lamb, M.P., de Leeuw, J., Fischer, W.W., Moodie, A.J., Venditti, J.G., Nittrouer, J.A., Hought, D., Parker, G., 2020. Mud in rivers transported as flocculated and suspended bed material. *Nat. Geosci.* 13, 566–570. <https://doi.org/10.1038/s41561-020-0602-5>.
- Le, H.-A., Gratiot, N., Santini, W., Ribolzi, O., Tran, D., Meriaux, X., Deleersnijder, E., Soares-Frazão, S., 2020. Suspended sediment properties in the Lower Mekong River, from fluvial to estuarine environments. *Estuar. Coast Shelf Sci.* 233, 106522 <https://doi.org/10.1016/j.ecss.2019.106522>.
- Li, G., Xu, K., Xue, Z.G., Liu, H., Bentley, S.J., 2021. Hydrodynamics and sediment dynamics in Barataria bay, Louisiana, USA. *Estuarine. Coastal and Shelf Science* 249, 107090. <https://doi.org/10.1016/j.ecss.2020.107090>.
- Mariotti, G., Ceccherini, G., McDonell, M., Justić, D., 2022. A comprehensive assessment of sediment dynamics in the Barataria Basin (LA, USA) distinguishes riverine advection from wave resuspension and identifies the Gulf intracoastal Waterway as a major sediment source. *Estuar. Coast* 45, 78–95. <https://doi.org/10.1007/s12237-021-00957-8>.
- Markussen, T.N., Andersen, T.J., 2013. A simple method for calculating in situ floc settling velocities based on effective density functions. *Mar. Geol.* 344, 10–18. <https://doi.org/10.1016/j.margeo.2013.07.002>.
- Meselhe, E., Sadid, K., Khadka, A., 2021. Sediment distribution, retention and morphodynamic analysis of a river-dominated deltaic system. *Water* 13, 1341. <https://doi.org/10.3390/w13101341>.
- Mietta, F., Chassagne, C., Manning, A.J., Winterwerp, J.C., 2009. Influence of shear rate, organic matter content, pH and salinity on mud flocculation. *Ocean Dynam.* 59, 751–763. <https://doi.org/10.1007/s10236-009-0231-4>.
- Mikeš, D., Manning, A.J., 2010. Assessment of flocculation kinetics of cohesive sediments from the seine and gironde estuaries, France, through laboratory and field studies. *J. Waterw. Port, Coast. Ocean Eng.* 136, 306–318. [https://doi.org/10.1061/\(ASCE\)WW.1943-5460.0000053](https://doi.org/10.1061/(ASCE)WW.1943-5460.0000053).

- Nepf, H.M., 2012. Flow and transport in regions with aquatic vegetation. *Annu. Rev. Fluid Mech.* 44, 123–142. <https://doi.org/10.1146/annurev-fluid-120710-101048>.
- Nghiem, J.A., Fischer, W.W., Li, G.K., Lamb, M.P., 2022. A mechanistic model for mud flocculation in freshwater rivers. *JGR Earth Surface* 127. <https://doi.org/10.1029/2021JF006392>.
- Nittrouer, J.A., Viparelli, E., 2014. Sand as a stable and sustainable resource for nourishing the Mississippi River delta. *Nat. Geosci.* 7, 350–354. <https://doi.org/10.1038/ngeo2142>.
- Osborn, R., Dillon, B., Tran, D., Abolfazli, E., Dunne, K.B.J., Nittrouer, J.A., Strom, K., 2021. FlocARAZI: an in-situ, image-based profiling instrument for sizing solid and flocculated suspended sediment. *JGR Earth Surface* 126. <https://doi.org/10.1029/2021JF006210>.
- Osborn, R., Dunne, K.B.J., Ashley, T.C., Nittrouer, J.A., Strom, K., 2023. The flocculation state of mud in the lowermost freshwater reaches of the Mississippi River: Spatial distribution of sizes, seasonal changes, and their impact on vertical concentration profiles. *J. Geophys. Res.: Earth Surf.* 128. <https://doi.org/10.1029/2022JF006975>.
- Ou, Y., Xue, Z.G., Li, C., Xu, K., White, J.R., Bentley, S.J., Zang, Z., 2020. A numerical investigation of salinity variations in the Barataria Estuary, Louisiana in connection with the Mississippi River and restoration activities. *Estuar. Coast Shelf Sci.* 245, 107021. <https://doi.org/10.1016/j.ecss.2020.107021>.
- Payandeh, A.R., Justic, D., Mariotti, G., Huang, H., Sorourian, S., 2019. Subtidal water level and current variability in a bar-built estuary during cold front season: Barataria bay, Gulf of Mexico. *J. Geophys. Res. Oceans* 124, 7226–7246. <https://doi.org/10.1029/2019JC015081>.
- Phillips, J.M., Walling, D.E., 1999. The particle size characteristics of fine-grained channel deposits in the River Exe Basin, Devon, UK. *Hydrol. Process.* 13, 1–19. [https://doi.org/10.1002/\(SICI\)1099-1085\(199901\)13:1<1::AID-HYP674>3.0.CO;2-C](https://doi.org/10.1002/(SICI)1099-1085(199901)13:1<1::AID-HYP674>3.0.CO;2-C).
- Rouse, H., 1937. Modern conceptions of the mechanics of fluid turbulence. *Transactions of the American Society of Civil Engineers* 102, 463–541.
- Salehi, M., Strom, K., 2011. Using velocimeter signal to noise ratio as a surrogate measure of suspended mud concentration. *Continent. Shelf Res.* 31, 1020–1032. <https://doi.org/10.1016/j.csr.2011.03.008>.
- Son, M., Hsu, T.-J., 2008. Flocculation model of cohesive sediment using variable fractal dimension. *Environ. Fluid Mech.* 8, 55–71. <https://doi.org/10.1007/s10652-007-9050-7>.
- Sorourian, S., Huang, H., Xu, K., Justic, D., D'Sa, E.J., 2022. A modeling study of water and sediment flux partitioning through the major passes of Mississippi Birdfoot Delta and their plume structures. *Geomorphology* 401, 108109. <https://doi.org/10.1016/j.geomorph.2022.108109>.
- Stapleton, K.R., Huntley, D.A., 1995. Seabed stress determinations using the inertial dissipation method and the turbulent kinetic energy method. *Earth Surf. Process. Landforms* 20, 807–815. <https://doi.org/10.1002/esp.3290200906>.
- Stein, S., Wingenroth, J., Larsen, L., 2021. A functional form for fine sediment interception in vegetated environments. *Geosciences* 11, 157. <https://doi.org/10.3390/geosciences11040157>.
- Strom, K., Keyvani, A., 2011. An explicit full-range settling velocity equation for mud flocs. *J. Sediment. Res.* 81, 921–934. <https://doi.org/10.2110/jsr.2011.62>.
- Swarzenski, C.M., 2003. Surface water hydrology of the GIWW in south-central Louisiana, 1672. USGS Prof. Pap.
- Swarzenski, C.M., Perrien, S.M., 2015. Discharge, suspended sediment, and salinity in the Gulf Intracoastal Waterway and adjacent surface waters in South-Central Louisiana, 1997–2008 (USGS Numbered Series No. 2015–5132), Scientific Investigations Report. U.S. Geological Survey, Reston, VA.
- Thill, A., Naudin, J.-J., Bottero, J.-Y., 2001. Evolution of particle size and concentration in the Rhone river mixing zone: influence of salt flocculation. *Continent. Shelf Res.* 21, 2127–2140.
- Turner, R.E., Swenson, E.M., Milan, C.S., Lee, J.M., 2019. Spatial variations in Chlorophyll a, C, N, and P in a Louisiana estuary from 1994 to 2016. *Hydrobiologia* 834, 131–144. <https://doi.org/10.1007/s10750-019-3918-7>.
- Verney, R., Lafite, R., Brun-Cottan, J.-C., 2009. Flocculation potential of estuarine particles: the importance of environmental factors and of the spatial and seasonal variability of suspended particulate matter. *Estuar. Coast* 32, 678–693. <https://doi.org/10.1007/s12237-009-9160-1>.
- Voulgaris, G., Meyers, S.T., 2004. Temporal variability of hydrodynamics, sediment concentration and sediment settling velocity in a tidal creek. *Continent. Shelf Res.* 24, 1659–1683. <https://doi.org/10.1016/j.csr.2004.05.006>.
- Walker, N.D., Wiseman Jr., W.J., R, L.J., Babin, A., 2005. Effects of River Discharge, Wind Stress, and Slope Eddies on Circulation and the Satellite-Observed Structure of the Mississippi River Plume. *J. Coast. Res.* 21, 1228–1244.
- Waterson, E.J., Canuel, E.A., 2008. Sources of sedimentary organic matter in the Mississippi River and adjacent Gulf of Mexico as revealed by lipid biomarker and $\delta^{13}C_{TOC}$ analyses. *Org. Geochem.* 39, 422–439. <https://doi.org/10.1016/j.orggeochem.2008.01.011>.
- Whitehouse, R., Soulsby, R., Roberts, W., Mitchener, H., 2000. Dynamics of estuarine muds. Thomas Telford Publishing.
- Wiberg, P.L., Sherwood, C.R., 2008. Calculating wave-generated bottom orbital velocities from surface-wave parameters. *Comput. Geosci.* 34, 1243–1262. <https://doi.org/10.1016/j.cageo.2008.02.010>.
- Winterwerp, J.C., 1998. A simple model for turbulence induced flocculation of cohesive sediment. *J. Hydraul. Res.* 36, 309–326. <https://doi.org/10.1080/00221689809498621>.
- Winterwerp, J.C., Manning, A.J., Martens, C., De Mulder, T., Vanlede, J., 2006a. A heuristic formula for turbulence-induced flocculation of cohesive sediment. *Estuar. Coast Shelf Sci.* 68, 195–207. <https://doi.org/10.1016/j.ecss.2006.02.003>.
- Winterwerp, J.C., Manning, A.J., Martens, C., de Mulder, T., Vanlede, J., 2006b. A heuristic formula for turbulence-induced flocculation of cohesive sediment. *Estuar. Coast Shelf Sci.* 68, 195–207. <https://doi.org/10.1016/j.ecss.2006.02.003>.
- Xu, K., Bentley, S., Robichaux, P., Sha, X., Yang, H., 2016. Implications of texture and erodibility for sediment retention in receiving basins of coastal Louisiana diversions. *Water* 8, 26. <https://doi.org/10.3390/w8010026>.
- Zang, Z., Xue, Z.G., Xu, K., Bentley, S.J., Chen, Q., D'Sa, E.J., Ge, Q., 2019. A two decadal (1993–2012) numerical assessment of sediment dynamics in the northern Gulf of Mexico. *Water* 11, 938. <https://doi.org/10.3390/w11050938>.
- Zhang, Q., Gong, Z., Zhang, C., Lacy, J.R., Jaffe, B.E., Xu, B., 2018. Bed shear stress estimation under wave conditions using near-bottom measurements: comparison of methods. *J. Coast Res.* 85, 241–245. <https://doi.org/10.2112/S185-049.1>.